POLVSM (Polarized Volume Scattering Meter) instrument: an innovative device to measure the directional and polarized scattering properties of hydrosols

Malik Chami, Alexandre Thirouard, Tristan Harmel

POLVSM (Polarized Volume Scattering Meter) instrument: an innovative device to measure the directional and polarized scattering properties of hydrosols

Malik Chami,[1,2,*] Alexandre Thirouard,[1] and Tristan Harmel[1]

[1]*Université Pierre et Marie Curie, CNRS, Laboratoire d'Océanographie de Villefranche, 181 Chemin du Lazaret, 06230 Villefranche sur Mer, France*

[2]*Institut Universitaire de France, 103 Boulevard Saint Michel, 75005 Paris, France*

[*]*chami@obs-vlfr.fr*

Abstract: An innovative instrument dedicated to the multispectral measurements of the directional and polarized scattering properties of the hydrosols, so-called POLVSM, is described. The instrument could be used onboard a ship, as a benchtop instrument, or at laboratory. The originality of the POLVSM concept relies on the use of a double periscopic optical system whose role is (i) to separate the plane containing the light source from the scattering plane containing the sample and the receiver and (ii) to prevent from any specularly reflected light within the sample chamber. As a result, a wide range of scattering angle, namely from 1° to 179°, is covered by the detector. Another originality of the instrument is to measure the Mueller scattering matrix elements, including the degree of polarization. A relevant calibration procedure, which could be of great interest as well for other instruments, is proposed to convert the raw data into physical units. The relative uncertainty in POLVSM data was determined at ± 4.3%. The analysis of measurements of the volume scattering function and degree of polarization performed under controlled conditions for samples dominated either by inorganic hydrosols or phytoplankton monospecific species showed a good consistency with literature, thus confirming the good performance of the POLVSM device. Comparisons of POLVSM data with theoretical calculations showed that Mie theory could reproduce efficiently the measurements of the VSF and degree of polarization for the case of inorganic hydrosols sample, despite the likely non sphericity of these particles as revealed by one of the element of the Mueller matrix. Our results suggested as well that a sophisticated modeling of the heterogeneous internal structure of living cells, or at least, the use of layered sphere models, is needed to correctly predict the directional and polarized effects of phytoplankton on the oceanic radiation. The relevance of performing angularly resolved measurements of the Mueller scattering elements to gain understanding on the mechanisms processes involved in the scattering of light by marine particles, which has important implications for ocean color remote sensing studies, is demonstrated.

OCIS codes: (010.4450) Oceanic optics; (120.4640) Optical instruments; (120.5820) Scattering measurements; (010.1350) Backscattering; (260.5430) Polarization.

References and links

1. M. Chami, D. McKee, E. Leymarie, and G. Khomenko, "Influence of the angular shape of the volume-scattering function and multiple scattering on remote sensing reflectance," Appl. Opt. **45**(36), 9210–9220 (2006).

#220922 - $15.00 USD Received 13 Aug 2014; revised 9 Oct 2014; accepted 9 Oct 2014; published 17 Oct 2014

2. J. E. Tyler and W. H. Richardson, "Nephelometer for the measurement of volume scattering function in situ," J. Opt. Soc. Am. **48**(5), 354–357 (1958).
3. T. J. Petzold, "Volume scattering functions for selected ocean waters," DTIC Document, 1972.
4. G. Kullenberg, "Observed and computed scattering functions," in *Optical Aspects of Oceanography* (Academic, 1974), pp. 25–49.
5. A. Morel, "Diffusion de la lumière par les eaux de mer. Résultats expérimentaux et approche théorique," Opt. Sea **63**, 1–76 (1973).
6. H. Volten, J. F. De Haan, J. W. Hovenier, R. Schreurs, W. Vassen, A. G. Dekker, H. J. Hoogenboom, F. Charlton, and R. Wouts, "Laboratory measurements of angular distributions of light scattered by phytoplankton and silt," Limnol. Oceanogr. **43**(6), 1180–1197 (1998).
7. M. E. Lee and M. R. Lewis, "A new method for the measurement of the optical volume scattering function in the upper ocean," J. Atmos. Ocean. Technol. **20**(4), 563–571 (2003).
8. B. Shao, J. S. Jaffe, M. Chachisvilis, and S. C. Esener, "Angular resolved light scattering for discriminating among marine picoplankton: modeling and experimental measurements," Opt. Express **14**(25), 12473–12484 (2006).
9. J. K. Lotsberg, E. Marken, J. J. Stamnes, S. R. Erga, K. Aursland, and C. Olseng, "Laboratory measurements of light scattering from marine particles," Limnol. Oceanogr. Methods **5**, 34–40 (2007).
10. M. E. Zugger, A. Messmer, T. J. Kane, J. Prentice, B. Concannon, A. Laux, and L. Mullen, "Optical scattering properties of phytoplankton: Measurements and comparison of various species at scattering angles between 1° and 170°," Limnol. Oceanogr. **53**(1), 381–386 (2008).
11. M. Babin, D. Stramski, R. A. Reynolds, V. M. Wright, and E. Leymarie, "Determination of the volume scattering function of aqueous particle suspensions with a laboratory multi-angle light scattering instrument," Appl. Opt. **51**(17), 3853–3873 (2012).
12. H. Tan, R. Doerffer, T. Oishi, and A. Tanaka, "A new approach to measure the volume scattering function," Opt. Express **21**(16), 18697–18711 (2013).
13. J. M. Sullivan and M. S. Twardowski, "Angular shape of the oceanic particulate volume scattering function in the backward direction," Appl. Opt. **48**(35), 6811–6819 (2009).
14. M. Twardowski, X. Zhang, S. Vagle, J. Sullivan, S. Freeman, H. Czerski, Y. You, L. Bi, and G. Kattawar, "The optical volume scattering function in a surf zone inverted to derive sediment and bubble particle subpopulations," J. Geophys. Res. **117**, C00H17 (2012).
15. W. H. Slade, Y. C. Agrawal, and O. A. Mikkelsen, "Comparison of measured and theoretical scattering and polarization properties of narrow size range irregular sediment particles," presented at *Oceans*, San Diego, (2013), 23–27.
16. M. Chami, "Importance of the polarization in the retrieval of oceanic constituents from the remote sensing reflectance," J. Geophys. Res. **112**, C05026 (2007).
17. A. Ibrahim, A. Gilerson, T. Harmel, A. Tonizzo, J. Chowdhary, and S. Ahmed, "The relationship between upwelling underwater polarization and attenuation/absorption ratio," Opt. Express **20**(23), 25662–25680 (2012).
18. G. W. Kattawar, "Genesis and evolution of polarization of light in the ocean," Appl. Opt. **52**(5), 940–948 (2013).
19. A. Gogoi, A. K. Buragohain, A. Choudhury, and G. A. Ahmed, "Laboratory measurements of light scattering by tropical fresh water diatoms," J. Quant. Spectrosc. Radiat. Transf. **110**(14–16), 1566–1578 (2009).
20. K. J. Voss and E. S. Fry, "Measurement of the Mueller matrix for ocean water," Appl. Opt. **23**(23), 4427–4439 (1984).
21. K. D. Lofflus, M. S. Quinby-Hunt, A. J. Hunt, F. Livolant, and M. Maestre, "Light scattering by Prorocentrum micans: a new method and results," Appl. Opt. **31**(15), 2924–2931 (1992).
22. K. Witkowski, L. Wolinski, Z. Turzynski, D. Gedziorowska, and A. Zielinski, "The investigation of kinetic growth of Chlorella vulgaris cells by the method of integral and dynamic light scattering," Limnol. Oceanogr. **38**(7), 1365–1372 (1993).
23. M. I. Mishchenko, J. W. Hovenier, and L. D. Travis, *Light Scattering by Nonspherical Particles: Theory, Measurements, and Applications* (Academic, 1999), p. 690.
24. M. Bressac, C. Guieu, D. Doxaran, F. Bourrin, K. Desboeufs, N. Leblond, and C. Ridame, "Quantification of the lithogenic carbon pump following a dust deposition event," Biogeosci. Discuss. **10**(8), 13639–13677 (2013).
25. E. Leymarie, D. Doxaran, and M. Babin, "Uncertainties associated to measurements of inherent optical properties in natural waters," Appl. Opt. **49**(28), 5415–5436 (2010).
26. M. S. Twardowski, E. Boss, J. B. Macdonald, W. S. Pegau, A. H. Barnard, and J. R. V. Zaneveld, "A model for estimating bulk refractive index from the optical backscattering ratio and the implications for understanding particle composition in case I and case II waters," J. Geophys. Res. **106**(C7), 14129–14142 (2001).
27. W. Zhou, G. Wang, Z. Sun, W. Cao, Z. Xu, S. Hu, and J. Zhao, "Variations in the optical scattering properties of phytoplankton cultures," Opt. Express **20**(10), 11189–11206 (2012).
28. H. Volten, O. Munoz, E. Rol, J. F. de Haan, W. Vassen, J. W. Hovenier, K. Muinonen, and T. Nousiainen, "Scattering matrices of mineral aerosol particles at 441.6 nm and 632.8 nm," J. Geophys. Res. **106**(D15), 17375–17401 (2001).
29. H. Volten, O. Munoz, J. W. Hovenier, J. F. de Haan, W. Vassen, W. J. Van der Zande, and L. Waters, "WWW scattering matrix database for small mineral particles at 441.6 and 632.8 nm," J. Quant. Spectrosc. Radiat. Transf. **90**(2), 191–206 (2005).

#220922 - $15.00 USD Received 13 Aug 2014; revised 9 Oct 2014; accepted 9 Oct 2014; published 17 Oct 2014

30. E. Aas, "Refractive index of phytoplankton derived from its metabolite composition," J. Plankton Res. **18**(12), 2223–2249 (1996).
31. R. W. Spinrad and J. F. Brown, "Relative real refractive index of marine microorganisms: a technique for flow cytometric estimation," Appl. Opt. **25**(12), 1930–1934 (1986).
32. M. Babin, D. Stramski, G. M. Ferrari, H. Claustre, A. Bricaud, G. Obolensky, and N. Hoepffner, "Variations in the light absorption coefficients of phytoplankton, nonalgal particles, and dissolved organic matter in coastal waters around Europe," J. Geophys. Res. **108**, 3211 (2003).
33. E. S. Fry and K. J. Voss, "Measurement of the Mueller matrix for phytoplankton," Limnol. Oceanogr. **30**(6), 1322–1326 (1985).
34. M. S. Quinby-Hunt, A. J. Hunt, K. Lofftus, and D. Shapiro, "Polarized-light scattering studies of marine Chlorella," Limnol. Oceanogr. **34**(8), 1587–1600 (1989).
35. R. D. Vaillancourt, C. W. Brown, R. R. L. Guillard, and W. M. Balch, "Light backscattering properties of marine phytoplankton: relationships to cell size, chemical composition and taxonomy," J. Plankton Res. **26**(2), 191–212 (2004).
36. M. W. Matthews and S. Bernard, "Using a two-layered sphere model to investigate the impact of gas vacuoles on the inherent optical properties of M. aeruginosa," Biogeosci. Discuss. **10**(6), 10531–10579 (2013).
37. O. Svensen, O. Frette, and S. R. Erga, "Scattering properties of microalgae: the effect of cell size and cell wall," Appl. Opt. **46**(23), 5762–5769 (2007).
38. A. L. Whitmire, W. S. Pegau, L. Karp-Boss, E. Boss, and T. J. Cowles, "Spectral backscattering properties of marine phytoplankton cultures," Opt. Express **18**(14), 15073–15093 (2010).
39. M. A. Yurkin, K. A. Semyanov, V. P. Maltsev, and A. G. Hoekstra, "Discrimination of granulocyte subtypes from light scattering: theoretical analysis using a granulated sphere model," Opt. Express **15**(25), 16561–16580 (2007).
40. M. A. Yurkin and A. G. Hoekstra, "The discrete-dipole-approximation code ADDA: capabilities and known limitations," J. Quant. Spectrosc. Radiat. Transf. **112**(13), 2234–2247 (2011).
41. M. I. Mishchenko, L. Liu, D. W. Mackowski, B. Cairns, and G. Videen, "Multiple scattering by random particulate media: exact 3D results," Opt. Express **15**(6), 2822–2836 (2007).
42. B. T. Draine and P. J. Flatau, "User guide for the discrete dipole approximation code DDSCAT 7.3," arXiv preprint arXiv:1305.6497 (2013).

1. Introduction

The angular distribution of the light scattered resulting from an incident beam interacting with an infinitesimally small volume of water is defined as the volume scattering function (VSF, hereafter noted $\beta(\theta)$ where θ is the scattering angle). The VSF is a fundamental inherent optical property (IOP) for determining the light field within the medium. In optical oceanography, the VSF is informative on the composition of suspended matter in the ocean (refractive index) and on their size distribution. It is a key function as well for ocean colour satellite remote sensing since it is directly related to the water leaving signal through the radiative transfer equation. Knowledge of the scattering directional properties of the ocean in the entire range of scattering angle (i.e., [0°-180°]) is theoretically required to predict the marine reflectance [1], which is of great interest for deriving biogeochemical properties of the water mass such as the phytoplankton biomass concentration. The first instruments dedicated to measurements of the VSF of marine samples were developed in the 1960s-1970s [2–5]. The concept of these instruments was based principally on either a light detector or a light source rotating around the sample volume. Since the late 1990s, a second generation of VSF instruments was built thanks to the significant advances made in the field of optical technology.

Two classes of instrument concepts are usually used to perform VSF measurements. Some instruments use a basin to store the sample (hereafter referred to as "basin concept" instruments) and other instruments work directly within the ocean (hereafter referred to as "in-situ concept" instruments). Most of the instruments that are currently available are based on the basin concept [6–12]. For such a concept, the water sample is placed within a basin and the detection of the scattered light is commonly performed in the same plane as the plane which contains the light source. The basin concept is convenient since it allows using the instrument as a benchtop one. The instrument is stabilized during a set of measurements, which is helpful as well to include some moving parts in the device. Furthermore, the overall size of the device is not a strong limitation in this type of concept, which is interesting to select the best optical/mechanical components regardless of their dimension. However, the

#220922 - $15.00 USD Received 13 Aug 2014; revised 9 Oct 2014; accepted 9 Oct 2014; published 17 Oct 2014

basin concept has constraints and limitations. The main limitation of the basin-concept relies on the difficulty to prevent the influence of the specular reflection of the incident beam onto the boundaries of the basin on the water sample. This reflected stray light induces a sharp increase of the VSF at backward scattering angles (e.g., typically from 150°). Such a problem could be overcome either by adopting a post-correction method [6, 11], by using a light trap system [10, 12] or by using a rotating customized prism [7]. For most of the basin-concept instruments, the light source is contained in the same plane as the beam that is measured by the detector [9–11]. As a result, the measurements of the VSF at high (typically > 160°) and weak (typically < 4°) scattering angles are made difficult. Typically, the light source masks the detector when this latter is positioned to measure the signal at high backscattering angles. Similarly, the optical components (e.g., lens, prisms, mirrors) could restrict the range of the measurements at low scattering angles. Lee and Lewis [7] proposed a periscopic optical system to guide the light into the basin to distinguish between the plane of the light source from the plane of detection. Using such a system, Lee and Lewis's instrument is able to measure the VSF within a wide range of scattering angle [0.6° to 177°]. Tan et al. [12] recently designed a relevant device based on cone reflectors to allow measurements at high scattering angles (up to 172°) but the sampling of the VSF at low scattering angles remains difficult (the measurements start at a scattering angle of 8°). Another constrain of basin-concept instruments relies on the fact that the propagation of light through media of various refractive indices (e.g., water/glass/air) induces a deformation of the scattered flux which could lead to significant angular errors in the measurements. Such a problem could be partially overcome either by surrounding the basin with a high refractive index medium like glycerin [6, 8, 9] or by reducing significantly the detector field of view [10, 11]. Note that the latter option leads to a loss of detected signal and thus, to a decrease of the sensitivity of the instrument.

The second class of VSF instrument that were developed, the "in-situ concept", consists of devices that are able to directly measure the angular distribution of the scattered light within the medium itself. This type of instrument does not require any basin to collect the water sample. Only a few of in situ concept VSF meters are currently available. The MASCOT device (Wetlabs Inc.) [13, 14] uses an array of several detectors, which are located in the same plane as a monochromatic light source, to measure the VSF in the range of scattering angle 10°-170°. The MASCOT concept is relevant to get a fast sampling of the VSF. In addition, there are no moving parts in the system. Both features contribute to make the instrument operational for a deployment at sea. However, one limitation of instruments using an array of detectors is that each detector needs to be calibrated properly to provide a consistent VSF measurement over the entire range of scattering angle. The LISST-VSF instrument (Sequoia Inc.) [15] uses a synergy of two original concepts to measure the VSF for a wide range of scattering angle, namely from 0.1° to 150°. The range of angles [0.1°-15°] is covered using a ring detector (same concept as the LISST instrument) while the angular range [15°-150°] is covered using a rotating eyeball detector. As it spins, the eyeball views scattering from different points (hence different angles) along the beam. The LISST-VSF is well designed to derive the total scattering coefficient of the water sample due to highly resolved angular measurements in the forward peak region. However, the derivation of the backscattering coefficient may not be so accurate due to the lack of data for scattering angles in the range 150°-180°.

Regardless of the concept used to build VSF instruments (basin-concept or in situ concept), they all need to detect a signal which vary within a wide dynamic range (typically 6 orders of magnitude between the forward peak and the backward scattering angles). Instruments using array of detectors [11, 13] could efficiently overcome this difficulty by adjusting the gain of each detector as a function of the range of scattering angle that is observed. Instruments using a single detector should either make sure the detector has a linear response over the entire domain of scattering angle [7] or modulate the light source power to

#220922 - $15.00 USD Received 13 Aug 2014; revised 9 Oct 2014; accepted 9 Oct 2014; published 17 Oct 2014

remain in the domain of linearity of the detector [10]. Recently, Tan et al. [12] interestingly proposed the use of a high sensitive CCD camera which does not require changes of sensitivity of the detector.

It has been shown the last decade that knowledge of the oceanic polarization state of light is of great interest for improving the retrieval of concentrations and/or optical properties of hydrosols. This is because polarized light is highly sensitive to the size, shape and composition of marine particles. Polarization is highly relevant as well to improve the performance of inverse algorithms dedicated to retrieve hydrosols optical and biogeochemical properties. As an example, Chami [16] investigated theoretically the influence of the marine particles upon the polarization state of the incident light. Chami [16] showed that the polarization properties of hydrosols could be used to distinguish between organic and inorganic matter. More recently, Ibrahim et al. [17] proposed a relevant theoretical relationship between the degree of polarization of the light and the inherent optical properties, namely the ratio between the attenuation coefficient versus the absorption coefficient. Other applications that demonstrate the interest of studying the polarized light characteristics in the ocean, such as the influence of the polarization on marine animal behavior, were described in details in Kattawar [18] and references therein. Therefore, measurements of the polarized VSF are thus required to gain understanding on the optical scattering mechanisms affecting the light in the ocean. Mathematically, the polarization properties of a given medium are entirely defined by the so-called 4x4 Mueller scattering matrix *M,* which is one of the main important inputs of vector radiative transfer models. Despite the importance of polarization light for various field of marine research (optics, biogeochemistry, biology), few instruments were able to measure the polarization features of hydrosols [6, 10, 15, 19–22]. Most of them either have a limited angular range (typically from 20° to 160°) or measure only few terms of the Mueller scattering matrix, namely the term M_{11} (VSF) and M_{12} (~degree of polarization). The majority of the instruments measuring the polarization were designed to perform laboratory measurements on phytoplankton cultures. The instrument used by Voss and Fry [20], which falls in the class of basin-concept instrument, was designed to measure natural samples onboard a ship. Only the instrument developed by Slade et al. [15] (i.e., the LISST-VSF) is currently able to carry out in situ measurements of the Mueller scattering matrix. Voss and Fry's instrument measured the full Mueller scattering matrix for scattering angles ranging from 10° to 160°. The LISST-VSF instrument, which is the only one that is currently commercially available, measures the three main terms of the matrix (M_{11}, M_{12}, M_{22}) only.

The objective of this paper is to describe a new instrument, so-called POLarized Volume Scattering Meter (POLVSM), that is able to measure the 3x3 Mueller scattering matrix of hydrosols, and thus their polarization properties. The instrument has been developed to overcome most of the limitations discussed above. Multispectral measurements are carried out for an angular range from 1° to 179° with a resolution of 1°. The POLVSM instrument works as a benchtop instrument that could be used either at the laboratory or onboard a ship. This paper is organized as follows. First, the instrument will be presented in details, including the data processing method and the calibration procedure. Then, experimental results obtained under controlled laboratory conditions for two types of hydrosols, namely inorganic and purely biogenic hydrosols, will be discussed.

2. POLVSM instrument

2.1 Theoretical background

The VSF $\beta(\theta)$ is mathematically defined as the second partial derivative of the scattered flux Φ with respect to solid angle Ω and the scattering volume V, normalized by the incident, collimated irradiance E [Eq. (1)]:

#220922 - $15.00 USD Received 13 Aug 2014; revised 9 Oct 2014; accepted 9 Oct 2014; published 17 Oct 2014

$$\beta(\theta) = \frac{\partial^2 \Phi(\theta)}{E \partial \Omega \partial V} \tag{1}$$

where θ is the scattering angle. The VSF is expressed in m^{-1} sr^{-1}. The volume of the scattering element can be decomposed as $\partial V = \partial A \partial r$ where A is the area perpendicular to the collimation axis of E and r is the thickness of the scattering element. As a result, β can be reformulated as a function of radiant intensity I as follows [Eq. (2)]:

$$\beta(\theta) = \frac{\partial I(\theta)}{E \partial r} \tag{2}$$

Based on Eq. (2), the scattering coefficient, b, and the backscattering coefficient, b_b, can be directly related to the VSF through Eq. (3) and Eq. (4) respectively:

$$b = \int_{\Omega} \beta(\theta) d\Omega = 2\pi \int_0^{\pi} \beta(\theta) \sin\theta d\theta \tag{3}$$

$$b_b = 2\pi \int_{\pi/2}^{\pi} \beta(\theta) \sin\theta d\theta \tag{4}$$

A beam light of arbitrary polarization can be represented by the Stokes vector $\mathbf{I} = (I,Q,U,V)^T$, the superscript T stands for the transpose of the vector. The first Stokes parameter, I, is informative of the total radiance (i.e., polarized and unpolarized part). The terms Q and U are informative of the linearly polarized radiance, and the term V stands for the circularly polarized radiance.

The scattering matrix describes the interaction between the incident beam with hydrosols within a sample. The Mueller scattering matrix M is defined based on the Stokes vector formalis, as the matrix which transforms an incident Stokes vector ***I*** into the scattered Stokes ***I'*** vector as follows [Eq. (5)]:

$$\mathbf{I}' = \begin{pmatrix} I' \\ Q' \\ U' \\ V' \end{pmatrix} = \mathbf{MI} = \begin{pmatrix} m_{11} & m_{12} & m_{13} & m_{14} \\ m_{21} & m_{22} & m_{23} & m_{24} \\ m_{31} & m_{32} & m_{33} & m_{34} \\ m_{41} & m_{42} & m_{43} & m_{44} \end{pmatrix} \begin{pmatrix} I \\ Q \\ U \\ V \end{pmatrix} \tag{5}$$

2.2 General principle of the POLVSM instrument

A schematic representation of the measurement principle of the Mueller scattering matrix elements by the POLVSM instrument is shown in Fig. 1. It should be first highlighted that the term V of the Stokes vector is not currently measured with the POLVSM instrument. Despite the fact that the magnitude of the term m_{44} could be quite similar as that of the term m_{33}, there is very little V in the marine environment. As a result, the impact of V on the polarization properties of marine particles remains minor relatively to the terms *I, Q* and *U*. The water sample is illuminated by several laser sources to measure the spectral Mueller matrix elements. The system is designed to collect measurements at six spectral bands in the best case. However, in this paper, the experiments were conducted in a configuration of three wavelengths (namely 440 nm, 532 nm and 660 nm). Each light source is placed on a translation table which moves after each monochromatic measurement to switch to another laser wavelength. The incident laser beam passes through an optical system which includes a polarizer, a beam expander and a mirror to reach a first prism P1 prior to entering a baffled chamber filled with the water sample. Note that a metalized mirror, namely a silver mirror (from Thorlabs Inc.), was used after the incident beam has been linearly polarized by a Glan-Thomson polarizer. Such type of mirror does not induce any polarization changes of the incident light when it is illuminated by a linearly polarized beam. The baffled chamber is a black cylindrical basin (volume of 1.5 litres) that is able to rotate around a vertical axis. Note

#220922 - $15.00 USD Received 13 Aug 2014; revised 9 Oct 2014; accepted 9 Oct 2014; published 17 Oct 2014

that the vertical axis of the basin crosses the direct incident beam at half distance of the total pathlength. The total pathlength is 7 cm for the POLVSM instrument. The direct light then propagates into the basin until a second customized prism P2 [Fig. 1(a)]. The role of the prism P2 is highly important since it is specifically designed first to guide the direct light outside the basin and second, to avoid any undesired backscattered light arising from the prism surface. The properties of the prism P2, which has been patented, will be further described with more details.

A small circular section of the basin has been cut as a window (glass planar surface) just behind the prism P2 to allow the measurement of the scattered light by a receiver. The receiver is thus positioned behind the window. The detection system is connected to the basin, ensuring a simultaneous rotation of both components. The receiver compartment is composed of rotating polarizer filters, a spectral filter, a convergent lens, diaphragms and a sensor that is positioned in the focal spot of the lens. The observation angle is determined by the angle between the pack "basin + detection" and the optical axis of the device (i.e., direct light pathway between prism P1 and P2) [Fig. 1(b)]. Note that the observation angle exactly corresponds to the scattering angle in such configuration. A complete measurement of the Mueller matrix of a given sample takes about 10 minutes in total. The user could regularly empty the basin and then fills it again to help the sample staying homogeneous.

2.3 Specification

2.3.1 The light source

High stability and high performance laser sources were used for the POLVSM device. The lasers power is 100 mW and the lasers output noise is 0.5%. The time drift is only 0.5% per 24 hours. The divergence of the light beam is less than 0.05° at half angle. Each laser source is totally linearly polarized in the direction of the vertical axis (y-axis) (i.e., angle of 90° from the reference x-axis). A rotating Glan-Thomson polarizer is however placed just after the laser source to ensure measurements at three polarization angles, namely 45°, 90° and 135° with respect to the x-axis. The rotating Glan-Thomson polarized will be hereafter referred to as the polarization state generator (PSG). A beam expander is placed as well in front of the laser sources to make homogeneous the beam diameters of each laser. A standard procedure is used to adjust the « zero angle » of the Glan Thomson polarizer. The rotation of this polarizer is performed and the angle for which the signal received by a second polarizer (which is in the receiver compartment of the instrument) is fairly zero (i.e., configuration of crossed polarizers) allows determining exactly the direction of polarization of the light entering into the basin.

2.3.2 The periscopic system

One of the main originality of the POLVSM concept relies on the use of a double periscopic optical system, which is composed of the mirror and the two prisms, that allows measurements, including in polarization, over a wider range of scattering angles (from 1° to 179°) than other instruments having a periscopic system too. Thanks to the POLVSM periscopic system, the propagation of the light is made from the light source to the detector in two parallel planes, namely the plane which contains the laser sources and the plane which contains the pack "basin + detector". On this basis, the scattering plane (i.e., the plane where the scattering processes within the sample happen) remains easy to determine [Fig. 1(a)].

The optical periscope allows the free rotation of the detector around the incident beam. As a result, the light source and the receiver do not obstruct each other. Because the light source is not physically disturbing the receiver, the shadow effect of the source is extremely reduced in the backward direction, especially for scattering angle greater than 160°. The VSF and the other Mueller scattering matrix elements could be thus measured up to 179° with the POLVSM instrument. Note that the reduction of the shadow effect induced by the light source

#220922 - $15.00 USD Received 13 Aug 2014; revised 9 Oct 2014; accepted 9 Oct 2014; published 17 Oct 2014

is one of the major challenges of the development of any VSF instruments as reminded in section 1.

The prism P2 of the periscopic system has been specifically customized to prevent any specular reflection of the incident beam onto the prism surface toward the water sample [Fig. 2]. This latter feature is highly important because the magnitude of such specularly reflected light could be sufficiently significant to generate additional undesirable scattering processes by hydrosols.

2.3.3 The sample compartment

The sample compartment is composed of a circular-shaped basin. An electro-chemical treatment based on the anodize process was applied to the surface of the basin to prevent any corrosion effects due to seawater. In addition, the anodizing process of the surface interestingly induces a change of color of the surface which becomes totally black, thus reducing efficiently the stray light reflection of the beam scattered by the marine particles onto the basin surface.

2.3.4 The receiver compartment

The receiver compartment of the POLVSM instrument includes a rotating polarizer filter, which is hereafter referred to as the polarization state analyser (PSA). The PSA is necessary to measure the scattered light at three polarization states for determining the nine elements of the Mueller scattering matrix. Note that the angles of rotation of the PSA, namely 30°, 90° and 150° with respect to the x-axis, are intentionally different from those used for the input polarizer PSG to prevent a total extinction of the light received by the detector.

Spectral filters, which are centered on the same wavelengths as those of the laser sources, are placed in front of the detector to measure exclusively the elastic scattering processes within the sample. Thus, the contribution of any effect of inelastic scattering within the sample (e.g., Raman or phytoplankton fluorescence) is removed.

A high performance photodiode Hamamatsu (S8745), which includes an amplifier, is used as the detector of the POLVSM device. Its noise equivalent power (NEP), which is informative on the minimum capacity of detection, is $1.1\ 10^{-15}$ W $Hz^{1/2}$. The signal to noise ratio of the photodiode is greater than 1000. Based on the sensitivity and on the dark noise level of the photodiode provided by the manufacturer, and thanks to an amplification custom made circuit as well, the lower limit of the detected power is estimated as 10^{-12} W. This value is consistent with the minimum power that should be sensed in the most critical configuration of the POLVSM instrument (i.e., crossed polarizers between the source and the detection). Note also that the linearity response of the photodiode is verified until such limit of detection. It should be highlighted that the minimum power sensed by the POLVSM instrument was calculated using the specifications of the instruments above described (i.e., laser power, pathlength, photodiode) for a minimum scattering coefficient value of 0.05 m^{-1} within the sample. A pinhole system was placed in front of the sensor to obtain an angular acceptance of 0.5°. Note that because the propagation of the incident beam received by the detector is systematically perpendicular to the surfaces encountered along its way (i.e., normal incidence), angular errors in the measurements are negligible in opposition to other systems which use cylindrical or spherical diopters [8]. The time constant of the detector is 0.1 second.

2.3.5 Sensitivity of the device to the polarization

To investigate the polarization properties of the water sample, the various optical components composing the POLVSM instrument should not alter the polarization state of the light scattered by hydrosols. Here, the fact that the incident beam propagates along the system through windows having a planar surface (thus with a normal incidence) allows maintaining the polarization state of the signal induced by hydrosols. Note also that the response of the detector is polarization independent.

#220922 - $15.00 USD Received 13 Aug 2014; revised 9 Oct 2014; accepted 9 Oct 2014; published 17 Oct 2014

2.3.6 Measurement of the scattered light at low scattering angles

One of the major challenging task when developing a volume scattering meter is to measure correctly the intensity of the light scattered at small scattering angles (i.e., in the forward peak). To perform measurements at very low scattering angles with the POLVSM instrument, the direct incident beam is adjusted to be as close as possible to the edge of the prism P2 during the phase of the alignment procedure of the overall optical system. Thus, the shadow effects induced by the prism P2 are highly minimised. The geometry of acquisition of the scattered beam at forward angles is shown in Fig. 3. Based on Fig. 3, the lowest value of the scattering angle θ_{min} for which the scattered light could be measured is calculated by Eq. (6):

$$\theta_{\min} = \arctan(\frac{2e}{D}) = 1° \quad (6)$$

where e is the distance between the direct incident beam and the edge of the prism P2 ($\sim 10^{-3}$ m), D is the distance between the two prisms (P1 and P2). As a result, the scattered light could be measured for a minimum theoretical value of scattering angle of 1°. The real minimum scattering angle that is measured by the instrument is determined experimentally during the alignment optical procedure which necessarily accounts for the beam diameter and profile. Note that the diameter of the lens composing the receiver compartment has been selected to ensure a collecting area sufficiently large in the case of small scattering angle to handle correctly the region of partial shadowing of the collector.

2.3.7 Influence of stray light in the POLVSM instrument

The influence of potential stray light is minimized over the entire POLVSM device for several reasons. First, the divergence of the incident laser beam is extremely weak. Second, high quality optical components having antireflection coatings are used. Third, the direct beam never propagates through any spherical dioptre along its pathway. The fact that the direct beam interacts only with planar surfaces is a key feature of the POLVSM design that considerably reduces the problems of stray light. Currently, other existing volume scattering meter instruments dedicated to laboratory measurements (e.g., Shao et al., 2006 [8]) have cylindrical tanks which induce significant reflection/refraction effects of the incident beam, thus restricting the angular range of the VSF measurements in both forward and backward direction (typically from >3° and more frequently > 10° up to 165°).

#220922 - $15.00 USD Received 13 Aug 2014; revised 9 Oct 2014; accepted 9 Oct 2014; published 17 Oct 2014

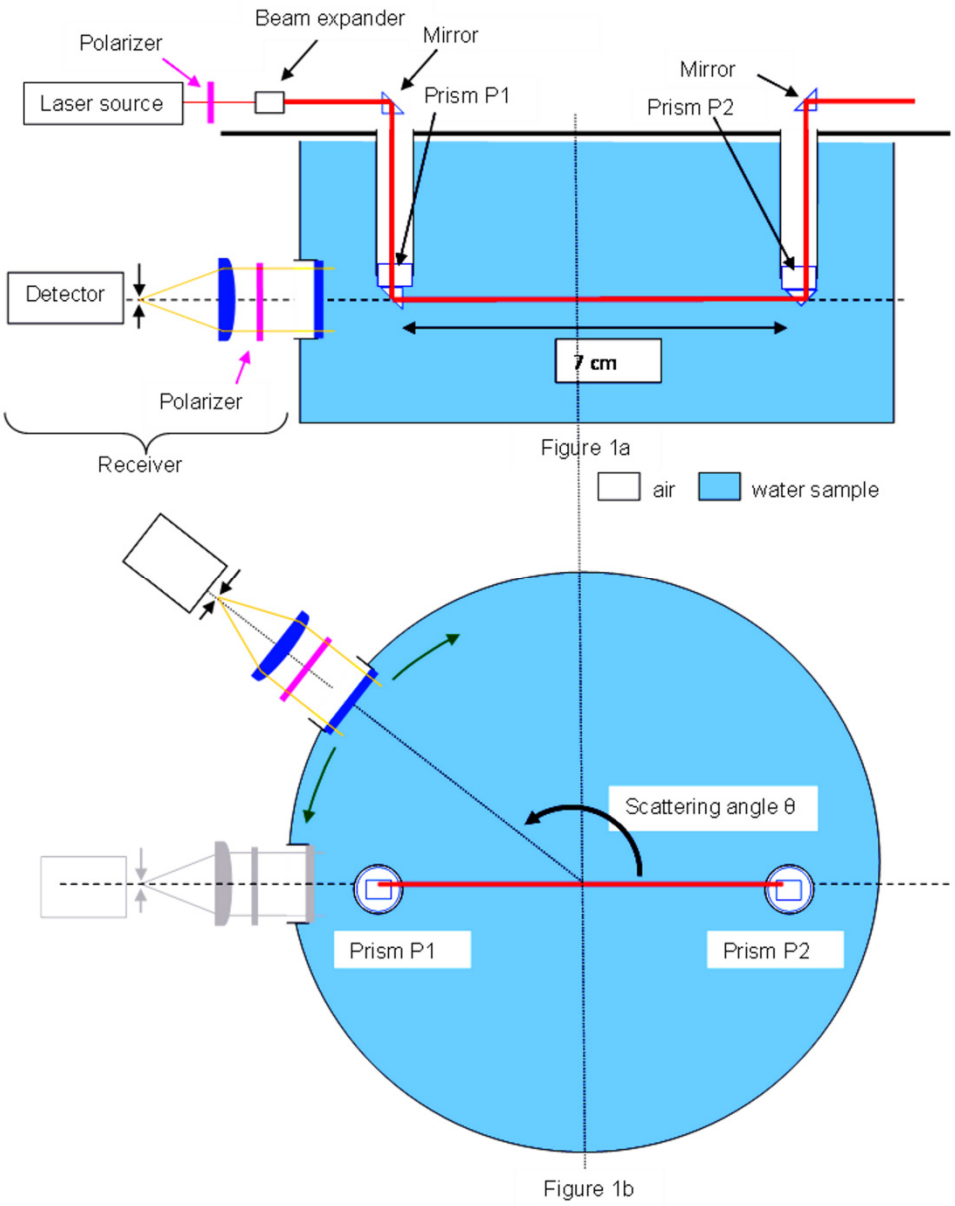

Fig. 1. A schematic representation of the measurement principle of the Mueller scattering matrix by POLVSM instrument: (a) side view, (b) view from above. Note that the prism P2 will be better illustrated in Fig. 2.

#220922 - $15.00 USD Received 13 Aug 2014; revised 9 Oct 2014; accepted 9 Oct 2014; published 17 Oct 2014

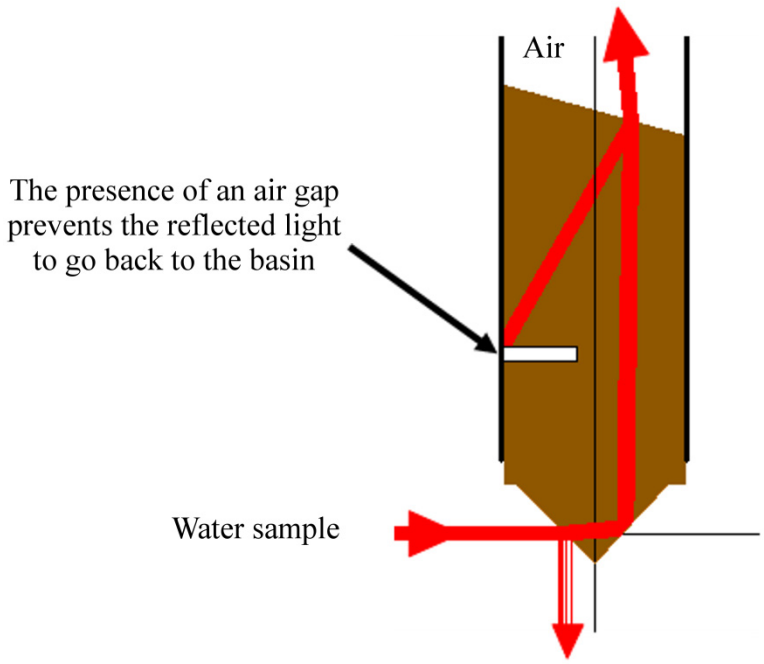

Fig. 2. Characteristics of the prism P2 of the optical periscope of the POLVSM instrument. The red beam represents the direct incident light within the sample. The prism P2 has been designed to prevent the specular reflection of the incident beam onto the prism surfaces to enter the basin. An air gap is created inside the prism to avoid the light reflected onto the top surface of the prism to go back to the basin.

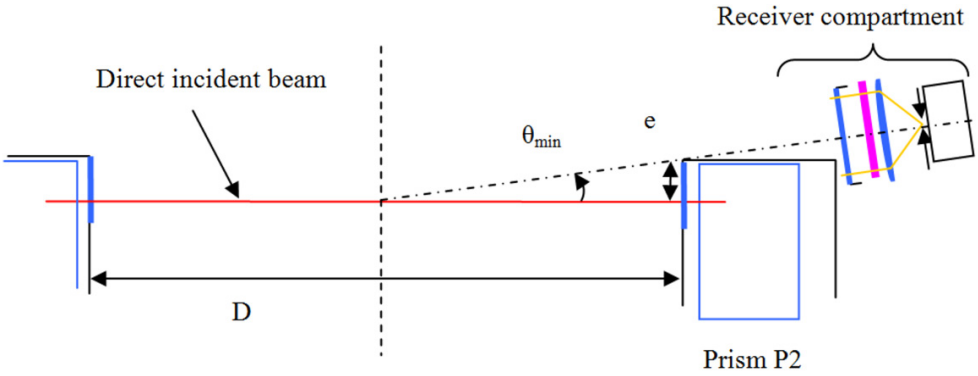

Fig. 3. Schematic representation (from above) of the geometry of acquisition of the scattered light by the receiver at small angles position. The optical system is aligned to make the incident direct beam touching the edge of the prism P2. The distance between the edge of the prism and the direct incident beam is noted *e*. The distance between the two prisms P1 and P2 is noted *D*. The angle θ_{min} is defined in Eq. (6).

3. Data processing

3.1 Inverse method

As described in section 2, the polarimetric configuration of the POLVSM device consists of four main components to measure the Mueller matrix: the light source, a polarization state

#220922 - $15.00 USD Received 13 Aug 2014; revised 9 Oct 2014; accepted 9 Oct 2014; published 17 Oct 2014

generator (PSG) placed just after the light source (here, the Glan-Thompson polarizer), the water sample, a polarization state analyser (PSA) placed just prior to the detector, and the detector itself. The PSG is used to set up the polarization state of the incident beam. The polarization state of the light scattered by the water sample is then analysed by the PSA prior to reaching the detector. To account for such polarimetric configuration, Eq. (5) is slightly modified as follows [Eq. (7)]. The scattered Stokes vector that is measured by the detector is then expressed:

$$\tilde{I}_{scat} = A * M * P * \tilde{I}_{inc} \tag{7}$$

where $\tilde{I}_{scat}$ is the scattered Stokes vector, $\tilde{I}_{inc}$ is the incident Stokes vector, M is the Mueller matrix of the sample, A and P matrices are the matrices of the PSA and PSG respectively. If α is referred to as the angle of rotation of a linear polarizer, the matrices $A(\alpha)$ and $P(\alpha)$ are expressed as follows [Eq. (8)]:

$$A(\alpha) = P(\alpha) = \frac{1}{2}\begin{pmatrix} 1 & \cos 2\alpha & \sin 2\alpha \\ \cos 2\alpha & \cos^2 2\alpha & \sin 2\alpha \cos 2\alpha \\ \sin 2\alpha & \sin 2\alpha \cos 2\alpha & \sin^2 2\alpha \end{pmatrix} \tag{8}$$

The detector is capable of measuring the first term I_{scat} of the Stokes vector $\tilde{I}_{scat}$ only. Considering all the polarimeter orientations, it is possible to write a system of equations from the corresponding I_{scat} measured by the detector. The resolution of this system of equations yields to the desired elements of the Mueller matrix M (see appendix for the full demonstration). As mentioned in section 2.3, the rotation of the PSG is performed successively at angles α = 45°, 90° and 135° (relatively to the x-axis) (see subsection *laser source*); the rotation of the PSA polarizer is performed successively at angles α = 30°, 90°, 150° (relatively to the x-axis) (see subsection *receiver compartment)*. Such a configuration ensures to correctly extract the nine elements of the matrix M.

3.2 Scattering volume correction and attenuation correction

To determine the Mueller matrix elements, knowledge of the scattering volume is required. The scattering volume is defined as the volume illuminated by the incident beam. It is necessary as well to correct both the incident and scattered beams for attenuation throughout the sample. Figure 4 shows a schematic top view of the POLVSM instrument configuration including the definition of the geometrical parameters. The procedure that is used here to perform both the scattering volume correction and the attenuation correction is outlined below. The following equations (Eqs. (9)-(16)) aim at calculating the transmission factor $T(\theta, c)$, where c is the attenuation coefficient of the sample, that should be applied to Eq. (7) to retrieve the Mueller matrix elements relatively to the POLVSM scattering volume.

The energy that is measured by the receiver compartment originates from a given length L along the incident beam pathway. For such configuration, the scattering volume could be determined by integrating the signal detected along the pathlength L. Based on Fig. 4, the length L could be expressed as follows [Eq. (9)]:

$$\begin{cases} L(\theta) = \dfrac{d}{\sin\theta}, \text{if } L(\theta) < D \\ L(\theta) = D, \text{otherwise.} \end{cases} \tag{9}$$

where d is the diameter of the converging lens and, D is the distance between the two prisms P1 and P2. The parameter D corresponds to the pathlength of the incident beam within the basin. Note that the scattering volume at 90° is 0.14 cm^3.

#220922 - $15.00 USD Received 13 Aug 2014; revised 9 Oct 2014; accepted 9 Oct 2014; published 17 Oct 2014

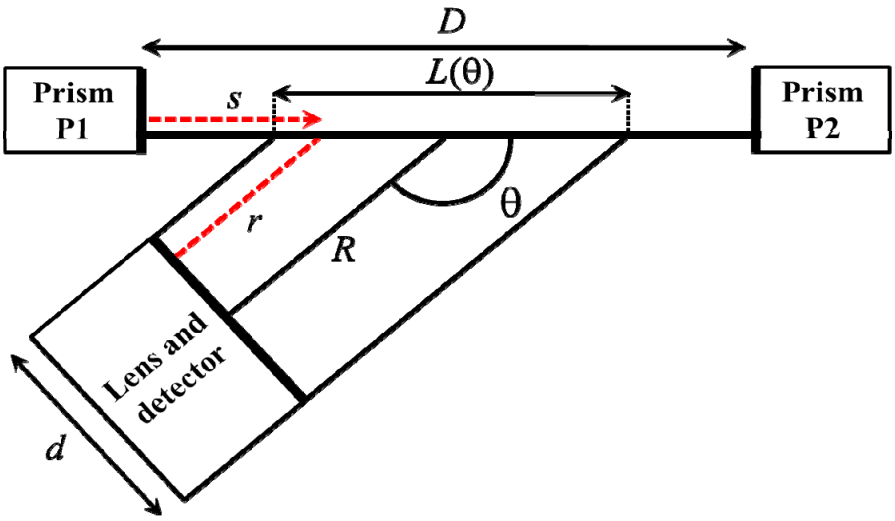

Fig. 4. Top view schematic representation of the POLVSM instrument configuration. All the geometrical parameters are defined as well.

Following the notations reported in Fig. 4, for a given polarimetric configuration of the PSA and PSG polarizers, the scattered signal I_{scat} originating from a point of the incident beam that is located at a distance s from the prism P1 and that reaches the receiver can be expressed as follows [Eq. (10)]:

$$I_{scat}(s) = e^{-c(s+r)} A * M * P * I_{inc} \tag{10}$$

Note that because the positions of the polarizers are fixed for a given measurement, the receiver measures a scalar signal and thus, the terms A and P in Eq. (10) correspond here to a line vector of dimension (1x3) and a column vector of dimension (3x1), respectively. The result obtained from Eq. (10) is then a scalar number.

The parameter r mentioned in Eq. (10) is expressed as follows [Eq. (11)]:

$$r = R + \left(\frac{D}{2} - s\right)\cos\theta \tag{11}$$

The total signal reaching the detector, hereafter noted as $I_{measured}$, is therefore the integral of I_{scat} over the length L [Eq. (12)]:

$$I_{measured} = \int_{s=\frac{D}{2}-\frac{L}{2}}^{\frac{D}{2}+\frac{L}{2}} I_{scat}\, ds = \int_{s=\frac{D}{2}-\frac{L}{2}}^{\frac{D}{2}+\frac{L}{2}} e^{-c(s+r)} A * M * P ds \tag{12}$$

Since the optical properties of the hydrosols are homogeneous within the basin (small volume), the Mueller matrix is assumed to be fairly constant along the path s. Eq. (12) could thus be written as follows [Eq. (13)]:

$$I_{measured} = A * M * P \int_{s=\frac{D}{2}-\frac{L}{2}}^{\frac{D}{2}+\frac{L}{2}} e^{-c(s+r)} ds = A * M * P * T \tag{13}$$

where T is a term which is related to the extinction of the signal along the path $s + r$. Note that the term T allows correcting for attenuation of the light along its pathway inside the scattering volume. The term T could be reformulated and determined as follows [Eq. (14) and Eq. (15)]:

#220922 - $15.00 USD Received 13 Aug 2014; revised 9 Oct 2014; accepted 9 Oct 2014; published 17 Oct 2014

$$T = \int_{s=\frac{D}{2}-\frac{L}{2}}^{\frac{D}{2}+\frac{L}{2}} e^{-c(s+r)} ds = e^{-c\left(R+\frac{D}{2}\cos\theta\right)} \int_{s=\frac{D}{2}-\frac{L}{2}}^{\frac{D}{2}+\frac{L}{2}} e^{-c\left(s(1-\cos\theta)\right)} ds \tag{14}$$

$$T(\theta,c) = \frac{2e^{-c\left(R+\frac{D}{2}\right)}}{c(1-\cos\theta)} \sin h\left(\frac{cL(1-\cos\theta)}{2}\right) \tag{15}$$

Finally, the Mueller matrix elements are determined for each scattering angle as follows [Eq. (16)] (see appendix):

$$M(\theta) = T(\theta,c)^{-1} A^{-1} I_{scat}(\theta) P^{-1} \tag{16}$$

As mentioned in Eq. (15), the attenuation coefficient c is required to calculate the term T. Since the POLVSM instrument does not have any sensor to measure the attenuation coefficient of the direct incident beam, an ancillary instrument should be used to measure c for the same sample. Practically, the coefficient c is measured using a standard beam transmission meter like the AC-9 Wetlabs instruments (Wetlabs Inc.).

3.3 Correction for pure water signal and for the apparatus function

Once the Mueller matrix of a sample has been retrieved using Eq. (16) for a given natural sample, it is necessary to obtain the Mueller matrix of the hydrosols only. The methodology consists of performing measurements for a sample containing pure water only, which is hereafter referred to as a "blank measurement". Note that this methodology is commonly used when dealing with instruments in the field of marine optics, such as AC9 instrument (Wetlabs Inc.). The idea of performing blank measurement is relevant for two reasons. First, the contribution for pure water signal to the total signal measured by the detector is removed, thus allowing the determination of the hydrosols contribution. Second, the apparatus function of the POLVSM instrument could be determined. Knowledge of the apparatus function is crucial to remove the various systematic artifacts due to the instrument itself. Blank measurements were performed using nanopure freshwater (Barnstead International Inc.). The corresponding Mueller matrix is noted M_{water}. Measurements are then carried out using the natural sample, which includes both pure water and hydrosols. The Mueller matrix of the sample, noted M_{sample} is then obtained. The Mueller matrix of the hydrosols, noted $M_{hydrosols}$, is then easily obtained by subtracting the contribution of the blank measurement from the sample data following Eq. (17):

$$M_{hydrosols}(\theta) = M_{sample}(\theta) - M_{water}(\theta) \tag{17}$$

To make sure that the removal of the blank water data does not influence the sensitivity of the POLVSM instrument to measure correctly the Mueller matrix elements of hydrosols, the contribution of the hydrosol signal to the total (hydrosol + blank water) signal was calculated for hydrosols having a scattering coefficient value of 0.05 m^{-1}, which is the lower limit of detection of the POLVSM device. Such a contribution was found to be 49%, 52%, 56%, 61% and 52% for the terms M_{11}, M_{12}, M_{21}, M_{22}, M_{33}, respectively. Therefore, the contribution of the hydrosols remains sufficiently significant relatively to the blank water contribution to ensure a correct detection of their Mueller matrix elements using the POLVSM instrument.

4. Calibration procedure and performance of the POLVSM instrument

The calibration procedure of the POLVSM instrument consists of converting the raw signal measured by the detector into geophysical units, namely m^{-1} sr^{-1}. The conversion factor is called the calibration coefficient. The calibration coefficient is supposed to be independent of the scattering angle. It should be highlighted that most of the VSF instruments that were

#220922 - $15.00 USD Received 13 Aug 2014; revised 9 Oct 2014; accepted 9 Oct 2014; published 17 Oct 2014

developed in the past (see section 1) were not calibrated to provide values into geophysical units due to the challenging task of such procedure. Yet, a successful calibration procedure highly contributes to assess the performance of an instrument. This section describes the different steps of the calibration methodology applied for the POLVSM device. Results and performance of the instruments are presented as well.

4.1 Calibration of the POLVSM instrument

The output signal of the POLVSM instrument was calibrated by measuring the VSF of a standard solution for which the magnitude of scattered light is known (in m^{-1} sr^{-1}). Note that the use of a single detector with a high degree of stability is a strength here relatively to instruments that use array of detectors, which require an additional intercalibration of the detectors each other.

Since the Mueller matrix elements other than the first term $M_{11,}$ namely $M_{i\neq1,j\neq1,}$ are commonly interpreted by normalizing them to the first term M_{11} [6, 19, 20], the calibration issue is thus reduced to the calibration of the single term M_{11}. As mentioned in Eq. (3), the integration of the term $M_{11}(\theta)$ (i.e., the VSF) over the scattering angle θ leads to the scattering coefficient b in m^{-1}. The calibration coefficient C_0, whose unit is in digital count*meter, could thus be theoretically determined as follows [Eq. (18)]:

$$C_0 = \frac{2\pi \int_{\theta=0}^{\pi} M_{11}^{uncal}(\theta)\sin\theta d\theta}{b_{known}} \tag{18}$$

where M_{11}^{uncal} is the uncalibrated output signal (in digital counts) received by the detector and b_{known} is the scattering coefficient of the sample that is supposed to be *a priori* accurately known.

Since the POLVSM instrument angular range of measurements [1°-179°] is not rigorously the full theoretical required range ([0-180°]), the integration of the terms involved in Eq. (18) should be carried out experimentally over the measured angular interval. This is not a problem because only the link between the output raw signal and the real magnitude of the total amount of scattering measured by the detector matters here. Therefore, the calibration coefficient C_0 is experimentally defined as follows [Eq. (19) and Eq. (20)]:

$$C_0 = \frac{2\pi \int_{\theta=\theta_{\min}}^{\theta_{\max}} M_{11}^{uncal}(\theta)\sin\theta d\theta}{b_{known}} \tag{19}$$

where θ_{min} and θ_{max} are respectively the lower and upper limit of the scattering angle measured by the POLVSM instrument; b_{known} is calculated from the integration of the VSF over the same angular interval [Eq. (20)].

$$b_{known} = 2\pi \int_{\theta_{\min}}^{\theta_{\max}} M_{11}^{known}(\theta)\sin\theta d\theta \tag{20}$$

Polystyrene microsphere beads of various sizes were employed for the calibration of the POLVSM instrument. As these artificial monodispersed particles are almost perfectly spherical with a precisely known size and refractive index, Mie theory calculations could be used to know exactly the magnitude of the scattering coefficient b_{known} of the sample. Therefore, b_{known} is first calculated theoretically using Mie theory using the specifications of the beads provided by the manufacturer. Then, the raw signal of the VSF is measured with the POLVSM instrument for a sample containing the same monodispersed population of beads. Here, the experiments were carried out for two beads size diameters, namely 1.0 µm and 3.0 µm. Table 1 summarizes the specifications of the beads that were used for the calibration

#220922 - $15.00 USD Received 13 Aug 2014; revised 9 Oct 2014; accepted 9 Oct 2014; published 17 Oct 2014

experiment. For both sizes, the beads refractive index relative to air was at 1.59 and their density was 1.05 g cm^{-3}. Note that the manufacturer provides the conversion factor to obtain the concentration in terms of number of the beads per cubic meter. Various concentrations of beads were used as well in our calibration experiments to obtain an uncertainty in the derived calibration coefficient. A reference concentration, noted $[N_1]$, was first fixed. Then, the reference concentration was multiplied by a given factor to fix the values of the other concentrations $[N_i]$. The concentration was varied up to 50 times higher than the reference value $[N_1]$ (Table 1).

Table 1. Specifications of the beads[a] used for the calibration experiments of the POLVSM instrument.

Size Diameter (in µm)	Beads Concentration $[N_i]$ (in Number per Cubic Meter)
1.0 µm	Reference Concentration: $[N_1] = 3.27\ 10^8$ $[N_2] = 2*[N_1]$; $[N_3] = 5*[N_1]$; $[N_4] = 10*[N_1]$; $[N_5] = 20*[N_1]$; $[N_6] = 50*[N_1]$
3.0	Reference Concentration: $[N_1] = 3.69\ 10^9$ $[N_2] = 2*[N_1]$; $[N_3] = 5*[N_1]$; $[N_4] = 10*[N_1]$; $[N_5] = 20*[N_1]$

[a] Microsphere beads; refractive index of 1.59 relative to air; density 1.05 g cm^{-3}

Table 2 presents the average value of the derived calibration coefficient C_{0mean} for each wavelength (i.e., λ = 440 nm, 532 nm, 660 nm). The standard deviation σ and the coefficient of variation CV (σ/C_{0mean}) (in %) are reported as well. The mean value of the coefficient of variation CV_{mean} calculated over the three spectral bands is informative on the overall relative uncertainty in the measurements of the POLVSM instrument.

As expected, the value of the calibration coefficient is wavelength dependent due to the spectral sensitivity of many of the optical components of the instrument. Note that the calibration coefficient for a given wavelength is supposed to be fairly independent of beads size, which was verified in our experiments. Table 2 shows that the coefficient of variation CV is less than 6.5% for all wavelengths. Based on the calibration experiments, the overall relative uncertainty in the measurement performed with the POLVSM instrument is 4.3% (i.e., CV_{mean}), which is very satisfactory considering the various sources of potential errors that could exist in any volume scattering meter instrument. It should be reminded that the uncertainty in the POLVSM instrument refers to natural samples for which the scattering coefficient is greater than 0.05 m^{-1} (see section 2.3).

Table 2. Average value of the calibration coefficient C_{0mean} (in digital counts*meter) and its standard deviation σ for each wavelength. The coefficient of variation (CV) is provided for each spectral bands. The mean value CV_{mean} represents an estimation of the overall relative uncertainty in the POLVSM data.

	Calibration Coefficients C_0 (in Digital Count * Meter)		
	λ = 440 nm	λ = 532 nm	λ = 660 nm
$C_{0mean} \pm \sigma$	$3.18 \pm 0.20*10^6$	$2.07 \pm 0.05*10^6$	$11.70 \pm 0.50*10^6$
$CV = \sigma/C_{0mean}$ (%)	6.29	2.42	4.27
CV_{mean} (%)		4.33	

Since the POLVSM data are acquired for the range of scattering angle [θ_{min} = 1°-θ_{max} = 179°], it is necessary to extrapolate the VSF measurements in the forward and backward direction respectively to really determine the scattering coefficient given his mathematical definition. Note, however, that because the VSF is weighted by a sinus function when calculating b (see Eq. (3)), whose function tends toward zero close to 0° and 180°, the impact of the extrapolations at very small and very large scattering angles on the calculation of b should be weak. In the forward direction, the VSF rapidly increases close to 0°. As a result, an exponential fit is performed to extrapolate the VSF near the forward peak° [Eq. (21)].

$$M_{11}(\theta) = M_{11}(\theta_{\min}) \exp(S_{forward} * \theta) \text{ if } \theta < \theta_{\min} \quad (21)$$

#220922 - $15.00 USD Received 13 Aug 2014; revised 9 Oct 2014; accepted 9 Oct 2014; published 17 Oct 2014

In the backward direction, a linear extrapolation is carried out from 179° to 180° because the shape of the VSF is not supposed to vary as sharply as at forward peak.

4.2 Angular validation of the POLVSM measurements

In addition to the determination of the calibration coefficient, it is necessary to check the consistency of the angular measurements to properly characterize the directional properties of hydrosols. For that purpose, each Mueller matrix element $M_{i,j}$ measured for beads experiments was compared with exact Mie theory calculations [Fig. 5].

Figure 5 shows the comparisons between the nine Mueller matrix elements simulated using Mie theory with the POLVSM measurements. Results are shown here for beads of diameter of 3.0 μm at wavelength 532 nm but similar results were obtained at other beads sizes and wavelengths. The term M_{11} was normalized by the scattering coefficient, thus corresponding to the so-called phase function (i.e, M_{11}/b). The other terms were divided by the term M_{11} to help the interpretation of the results. It is observed that the POLVSM data closely follow the angular structure of Mie theory calculations for each Mueller matrix elements. Interestingly, the measured phase function satisfactorily matches with theory including at high backward angles ($\theta > 160°$). POLVSM data remain consistent with theory up to the maximum limit of the measured scattering angle, namely 179°. As mentioned earlier (section 1), such a range of scattering angles is particularly difficult to measure accurately with volume scattering meter instruments. Therefore, Fig. 5 confirms the efficiency of the special design of the prism P2 [Fig. 2]. It should be highlighted that the use of such prism P2 could be helpful for the development of other kinds of instruments for which undesirable backscattered light toward a detector needs to be removed. Figure 5 also illustrates that the measured degree of polarization, namely the term M_{12}/M_{11}, is highly consistent with theory. This result demonstrates the relevance of the POLVSM design to analyze the polarization properties of hydrosols. Note that the crossed terms M_{21}/M_{11} and M_{12}/M_{11} are equal as expected from theory [23]. The term M_{22}/M_{11} is usually informative on the shape of the particles. Figure 5 shows that the ratio M_{22}/M_{11} is fairly equal to unity as expected for spherical particles. The measured off-diagonal terms M_{13}, M_{23}, M_{31}, M_{32} are close to zero, which is consistent again with simulations. The term M_{33}/M_{11}, which is informative on the direction of the polarization of the electric field, is satisfactorily measured. The element M_{33}/M_{11} is much more difficult to interpret in terms of scattering mechanisms induced by the hydrosols than the other terms such as the degree of polarization. For that reason, we will mainly focus in the rest of this current study on the interpretation of the terms M_{11}, M_{12}/M_{11} and M_{22}/M_{11}.

#220922 - $15.00 USD Received 13 Aug 2014; revised 9 Oct 2014; accepted 9 Oct 2014; published 17 Oct 2014

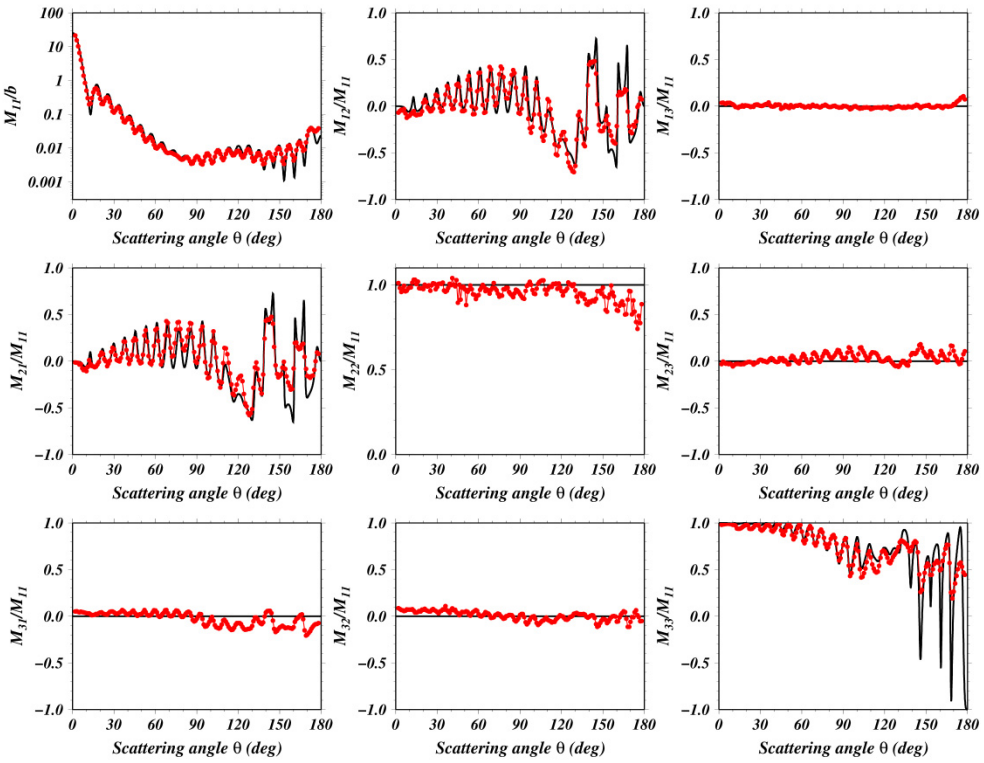

Fig. 5. Comparison of the nine Mueller matrix elements measured using the POLVSM instrument during a calibration experiment at 532 nm with Mie theory calculations. Microsphere beads of diameter 3.0 µm were used (see Table 1 for the specifications of the beads). The term M_{11} has been normalized to the scattering coefficient to get the phase function. The other matrix elements were divided by the term M_{11} to help the interpretation of the data. For example, the term M_{12}/M_{11} corresponds to the degree of polarization of the beads.

The uncertainties in the ratios M_{12}/M_{11}, M_{21}/M_{11}, M_{22}/M_{11} and M_{33}/M_{11} were quantified through the experiments with beads. For that purpose, comparisons between the measurements with Mie theory were performed over the entire angular range Note that since the ratios of some terms of the matrix, namely M_{13}/M_{11}, M_{23}/M_{11}, M_{31}/M_{11}, M_{32}/M_{11}, are systematically close to zero, it is not really relevant to determine their uncertainty. The uncertainties were determined as follows. For each ratio, the normalized root mean square error ($NRMSE_p$, in %) was calculated based on Eq. (22) for each experiment p (i.e., for a given beads size and concentration) to quantify the differences over the entire range of scattering angles between data and theory.

$$NRMSE_p = \frac{\sqrt{\frac{1}{n}\sum_{k=1}^{n}\left(\tilde{M}_{i,j,measured}(\theta_k) - \tilde{M}_{i,j,theory}(\theta_k)\right)^2}}{\tilde{M}_{i,j,theory,\max} - \tilde{M}_{i,j,theory,\min}} \qquad (22)$$

In Eq. (22), n is the number of scattering angles, $\tilde{M}_{i,j}(\theta_k)$ is the ratio $M_{i,j}/M_{11}$ for the beads experiment p at the scattering angle θ_k, $\tilde{M}_{i,j,theory,\max}$ and $\tilde{M}_{i,j,theory,\min}$ are respectively the maximum and minimum values of the ratio over the angular range of data. It should be stressed that the $NRMSE$ is an appropriate metric when the analyzed function could have some values close to zero over the range of data, as it could be the case here for the ratios $M_{i,j}/M_{11}$ at certain scattering angles. The $NRMSE_p$ values were then averaged over all the

#220922 - $15.00 USD Received 13 Aug 2014; revised 9 Oct 2014; accepted 9 Oct 2014; published 17 Oct 2014

experiments p to provide the uncertainty $NRMSE_{mean}$ in the terms $M_{i,j}/M_{11}$ (Table 3). It is observed that the uncertainties in the various terms are are about 10% (Table 3), which remains satisfactory.

Table 3. Uncertainties in the main terms $M_{i,j}/M_{11}$ of the Mueller matrix.

	M_{12}/M_{11}	M_{21}/M_{11}	M_{22}/M_{11}	M_{33}/M_{11}
$NRMSE_{mean}$(in %)	10.3	10.4	8.7	8.8

In summary, it is clear from Fig. 5 and Table 3 that the experimental setup and data handling of the POLVSM instrument lead to a scattering structure of the measurements that accurately reflects that found in theory. This setup can be expected to provide equally accurate results in experimental scattering targets. Of course, natural suspensions will likely have less structure in their scattering functions, as it will be discussed in section 5, mainly because of the polydispersion of hydrosols. Since the angular shape of the Mueller matrix elements of polydisperse hydrosols (as it could be observed in natural samples) is usually smooth from one scattering angle to another, it should be highlighted that potential spikes in the data could be easily removed by applying moving window filters over given intervals of scattering angles.

5. Experimental results

Figure 6 shows the experimental scattering results of the VSF and the degree of polarization for polydispersed suspensions of hydrosols under controlled conditions at the laboratory. Measurements were carried out for two relevant cases. One sample consisted of purely inorganic hydrosols while the other sample consisted of purely biogenic hydrosols. The first sample contained a mineral-like suspension, which was prepared using aerosols collected in the Sahara desert (Africa) by the laboratory "Laboratoire Interuniversitaire des Systèmes Atmosphériques (LISA)" (Université Paris-Est Créteil, France). The protocol for collecting aerosols is described in Bressac et al. [24]. It should be highlighted that dust aerosols deposit is frequently observed in oceanic waters such as the Mediterranean Sea or the Atlantic Ocean [23]. The aerosols were then diluted into pure seawater. It should be highlighted that the dust aerosols used here showed a yellow-brown color. The second sample contained the phytoplankton species *Pseudo-nitzschia,* which was grown at the laboratory "Laboratoire d'Océanographie de Villefranche" (LOV)" (Université Pierre et Marie Curie, France). The size distributions of the particles were measured using a Coulter Counter. It was observed that the mineral-like particles were distributed according to a Junge power law with a slope value of 3.4. The mean radius of the mineral-like particles was 0.7 μm. The size distribution of the sample containing the phytoplankton species followed a lognormal function with a mean radius value of 2.96 μm and a variance of 0.187 μm^2.

#220922 - $15.00 USD Received 13 Aug 2014; revised 9 Oct 2014; accepted 9 Oct 2014; published 17 Oct 2014

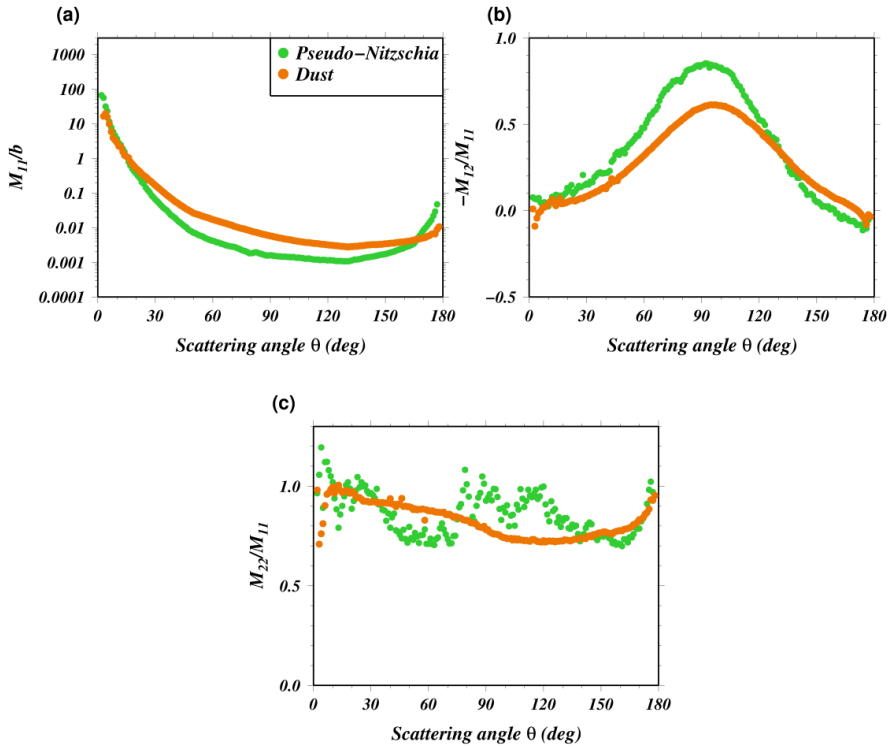

Fig. 6. Experimental results of three Mueller scattering matrix elements at 440 nm for two different polydispersed suspensions, namely mineral dust-like particles (brown dots) and the phytoplankton species *Pseudo-nitzschia* (green dots) under controlled laboratory conditions: (a) phase function (i.e., term M_{11}/b), (b) degree of polarization (i.e., term M_{12}/M_{11}), (c) ratio M_{22}/M_{11}.

Figure 6(a) shows that the shape of the VSF for both samples is much smoother over all the range of scattering angles than that observed for monodispersed beads [Fig. 5]. This was expected due to the higher polydispersion of particulates within the samples relative to beads experiments. It is interesting to observe a different shape of the VSF in the backward direction. The biogenic hydrosol *Pseudo-nitzschia* shows a significant increase of the VSF by more than one order of magnitude in the range of scattering angle [150°-180°]. A sharp increase of the VSF that could reach similar order of magnitude in such backward direction has been previously observed in the literature for various phytoplankton species [12]. Field observations in oligotrophic natural waters like those found in the Pacific Ocean [20] showed as well a sharp increase of the VSF at high scattering angles. The Pacific Ocean waters are likely mostly dominated by phytoplankton type particles rather than mineral-like particles due to the lack of terrestrial river inputs or strong aerosol deposits there. The VSF of mineral-like hydrosols as observed in our experiment do not exhibit a sharp increase of the VSF in this region. Such a fairly flat variation of the VSF in the backward direction of this type of hydrosols is consistent with recent observations carried out in coastal zone sediment-dominated waters using MASCOT instrument [14]. From a more technical point of view, the measurements shown in Fig. 6(a) illustrate that the POLVSM instrument does not produce any systematic bias at high scattering angles since highly different behaviors of the VSF (increase or fairly flat variation when $\theta > 160°$) are observed. These results corroborate again the efficiency of the role played by the prism P2 to prevent some stray light reflection toward the detector when hydrosols other than perfect beads are used.

#220922 - $15.00 USD Received 13 Aug 2014; revised 9 Oct 2014; accepted 9 Oct 2014; published 17 Oct 2014

The measurement of the VSF with POLVSM instrument allows calculating the particulate backscattering ratio $\tilde{b}_{bp}$, which is defined as the particulate backscattering coefficient b_{bp} divided by the particulate scattering coefficient b_p. $\tilde{b}_{bp}$ is an important optical parameter that is dependent on the composition (i.e., refractive index) and the size of the particles. It plays an important role as well for satellite remote sensing studies since it is informative on the efficiency of particles to backscatter light toward the sea surface. The scattering coefficients of our phytoplankton-dominated and inorganic-dominated samples were 1.05 m^{-1} and 2.19 m^{-1} respectively. Note that these values were in agreement with AC9 data within 10%, which is satisfactory considering the uncertainties in the data acquired by devices that use similar concept as the AC9 instrument [25]. The values of the backscattering ratio derived here for the phytoplankton species *Pseudo-nitzschia* and the mineral-like particles were 0.44% and 1.2% at 440 nm respectively. Low values of $\tilde{b}_{bp}$ (typically lower than 1%) are expected for biogenic hydrosols because of their low refractive index (close to the pure seawater refractive index) and sometimes, because of their large size [26]. Zhou et al. [27] reported a backscattering ratio of 0.38% for the same phytoplankton species. Thus, the value obtained using POLVSM instrument for the species *Pseudo-nitzschia* is consistent with literature. One could think as well that their large size (mean radius of 2.9 µm in our experiment) induce a strong diffraction of the light near the forward peak which result in a weak backscattering efficiency. The backscattering ratio derived for inorganic hydrosols (~1.2%) seems a little bit low compared to what one could expect based on their potential higher refractive index and smaller size (mean radius of 0.5 µm here) relatively to biogenic hydrosols. The consistency of the backscattering ratio value measured for inorganic hydrosols with ancillary data will be discussed later in the paper (section 6).

Figure 6(b) shows the variation of the degree of polarization (i.e., M_{12}/M_{11}) at 440 nm with respect to the scattering angles for the biogenic and inorganic hydrosols. A bell-shape of the degree of polarization is observed with a maximum peak around 90°. Such a bell-shape is consistent with previous laboratory measurements carried out by Volten et al. [28] and Zugger et al. [10] for various phytoplankton species. A bell-shape could be expected as well for our mineral-like sample as it is frequently observed when dealing with aerosols particles [29], which contribute to the major particulate component of our inorganic sample. The maximum value of the degree of polarization is about 80% for *Pseudo-nitzschia* while it is about 50% for inorganic hydrosols. It is well known that the degree of polarization decreases with increasing refractive index relative to water. Since the refractive index of biogenic hydrosols which is typically in the range of 1.04 to 1.09 [30, 31] is much closer to water than that of inorganic particles, which is typically in the range [1.10-1.25] [32], it is thus consistent to observe a stronger polarizing properties of *Pseudo-nitzschia* than that of inorganic material. Furthermore, previous studies showed similar strong values (~80%) of M_{12}/M_{11} for phytoplankton species [33, 34] or for natural ocean water samples [20]. However, this latter comment needs to be moderated by the fact that the particle size distribution could strongly influence as well the maximum value of the degree of polarization. In particular, very small particles induce a much stronger polarization of the radiation than large particles. Therefore, the value of the degree of polarization is the result of the balance between the size and the composition of the hydrosols. Here, since the mean radius of our inorganic particles is much lower (0.5 µm) than that of the phytoplankton species (2.9 µm), it seems that the refractive index of the particles mostly drives the variation of M_{12}/M_{11}.

Figure 6(c) shows the angular variation of the Mueller scattering matrix element M_{22}/M_{11} at 440 nm. This term is informative on the shape of the particles present in the sample. Typically, M_{22}/M_{11} is equal to unity for perfect spherical particles. A deviation from unity means a more complex shape of the particles such as spheroidal, cylindrical or elliptical shape. Note that measurements of the term M_{22}/M_{11} for hydrosols are rarely found in the

#220922 - $15.00 USD Received 13 Aug 2014; revised 9 Oct 2014; accepted 9 Oct 2014; published 17 Oct 2014

literature dealing with ocean optics field research. The angular variation of this element shows a significant departure from unity [Fig. 6(c)], by almost 25% for both the inorganic hydrosols and *Pseudo-nitzschia* phytoplankton species. It is not so surprising to observe a fairly strong deviation of the hydrosols shape from spheres. However, as it will be discussed later (section 6), such observation does not mean necessarily that the scattering theory (like Mie theory) which is dedicated for spherical particles is not applicable to retrieve the scattering properties of non-spherical hydrosols.

6. Discussion

To gain some understanding on the directional and polarized properties of the hydrosols for which the Mueller matrix elements were measured in this paper, comparisons with Mie theoretical calculations of the VSF and degree of polarization were carried out. Despite the fact that the shape of the hydrosols used in this study is not spherical (see Fig. 6(c), term M_{22}/M_{11}), Mie theory could be useful to understand some of the scattering mechanisms of marine particles. Note that comparisons with Mie theory has been commonly used by several authors [6, 10] for similar type of analysis.

The VSF measurements of mineral-like hydrosols [Fig. 6(a)] revealed a relatively low value of backscattering ratio (1.2%) compared to what could be expected for inorganic matter. To verify the consistency of our POLVSM data, Mie calculations were performed to predict the VSF of particles having similar optical features. Since the aerosols that were introduced to the seawater sample are dusts-like particles, the refractive index of our inorganic hydrosols was assumed to be pretty similar as that found for Saharan dust optical properties. Volten et al. [28] reported a value of refractive index of 1.5 relative to air (see their Table 1) for Saharan dust showing a yellow-brown color. Therefore, a refractive index of 1.12 relative to water was used to model our inorganic hydrosols with Mie theory. The same Junge power law size distribution with a slope value of 3.4 as it was measured during our experiments was used. Based on these realistic model inputs, the VSF was simulated and compared with POLVSM data [Fig. 7(a)]. The comparison shows that the modelled values nicely reproduce the measurements. Such a good agreement tends to confirm that a backscattering ratio close to 1.2%, as observed by POLVSM instrument, could make sense when dealing with inorganic suspended matter that originates from dust composition. Note that our computations are consistent as well with those obtained by Twardowski et al. [26]. The Mie modeling results satisfy fairly well the measured degree of polarization [Fig. 7(b)]. Such an agreement is surprising due to the non-sphericity of the inorganic hydrosols as previously illustrated by the departure of M_{22}/M_{11} from unity [Fig. 6(c)]. The good match between theoretical simulations and VSF and degree of polarization measurements suggest that our inorganic hydrosols are likely sufficiently homogeneous in their internal structure and sufficiently randomly oriented in space as well to be considered as optically equivalent to spheres in terms of their scattering properties despite their non spherical real shape. Mie theory could thus be applied to reproduce the scattering directional and polarized features of non spherical hydrosols under given circumstances. However, a caution should be made that these results might not be generalized to all kinds of inorganic hydrosols due to their great variability in their composition and in their subsequent scattering directional properties.

The comparisons between Mie calculations and POLVSM data for the phytoplankton species *Pseudo-nitzschia* do not exhibit similar results as those obtained for the case of inorganic material [Fig. 7(c) and Fig. 7(d)]. For such living cells, it is difficult to retrieve properly the VSF and degree of polarization measurements using Mie theory despite the fact that realistic parameters were used as inputs (i.e., measured lognormal size distribution with a mean radius of 2.9 µm and a complex refractive index of 1.04-0.0038i following Zhou et al.'s study [27]). In particular, the maximum value of the degree of polarization differs by almost a factor of 2. A high discrepancy is observed as well for the VSF especially for scattering angles greater than 90° where the simulation shows a much flatter angular shape of the VSF

#220922 - $15.00 USD Received 13 Aug 2014; revised 9 Oct 2014; accepted 9 Oct 2014; published 17 Oct 2014

than that of the measurements. Such discrepancy is verified when comparing the backscattering ratio values between the simulation and the data. The backscattering ratio of Mie calculation is 0.054% which is about one order of magnitude lower than our measurements. A similar difference in the magnitude of the backscattering efficiency of phytoplankton retrieved between modelling results and data was previously observed by Vaillancourt et al, 2004 [35]. Note that Volten et al. [6] also concluded that it is often difficult to reconcile measurements with theory for living phytoplankton. The discrepancies observed here might not be solely explained by the fact that *Pseudo-nitzschia* departs from the spherical shape. They may be explained as well by the fact that the internal structure of living cells could be highly complex. It has been shown that the heterogeneity of the different structures composing phytoplankton cells could induce complex scattering mechanisms inside the cells itself, which could potentially alter the overall scattering of the light outside the cell [36–38]. Figure 7(d) finally confirms the requirement to develop and/or to use much more sophisticated numerical tools than Mie theory for modeling the internal structures of living cells to simulate realistically their scattering and polarized properties. Complex models that account for the heterogeneity of the internal structures of living cells currently exist [39–42]. At least, the use of layered sphere models for which a variation of the refractive index is applied might improve the model-data polarization comparison for phytoplankton cells. It is not the scope of this paper to investigate this aspect which should be treated in a future work. In any case, the mismatch observed in this study between Mie theory and POLVSM measurements for phytoplankton species demonstrates the great potential of using polarization-based nephelometers to characterize the directional effects of hydrosols.

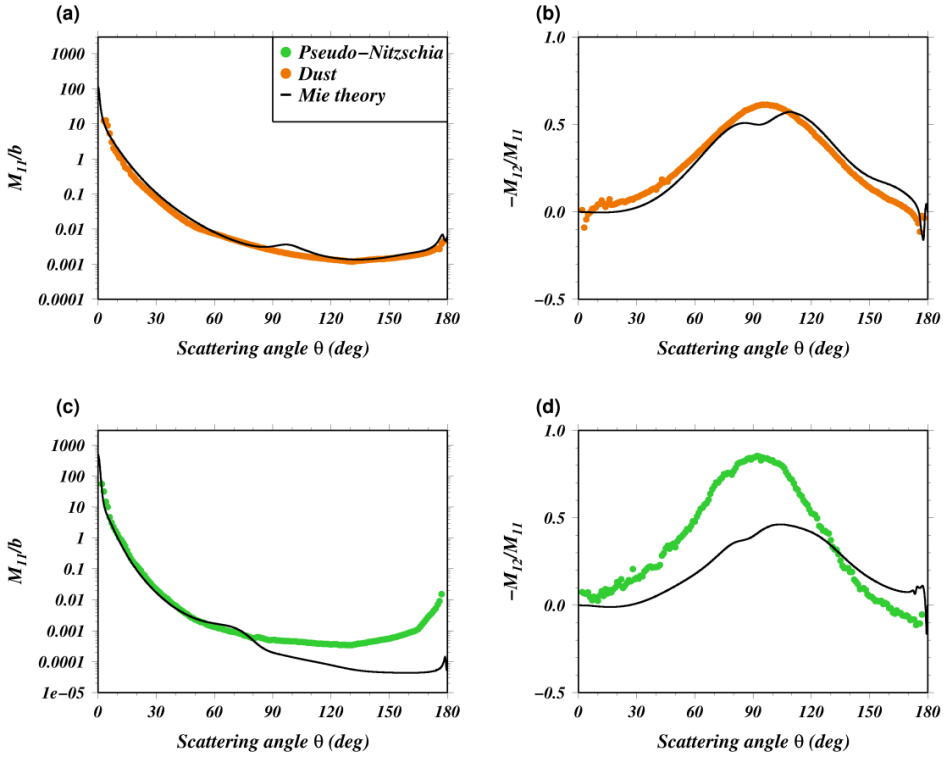

Fig. 7. (a) Comparison between VSF measurements of inorganic dust-like hydrosols (POLVSM data, dotted line) with Mie theory (solid black line), (b) comparison of the degree of polarization (M_{12}/M_{11}) of inorganic dust-like hydrosols (POLVSM data, dotted colored line) with Mie theory (solid line), (c) same as Fig. 7(a) but for phytoplankton species *Pseudo-nitzschia*, (d) same as Fig. 7(b) but for phytoplankton species *Pseudo-nitzschia*.

#220922 - $15.00 USD Received 13 Aug 2014; revised 9 Oct 2014; accepted 9 Oct 2014; published 17 Oct 2014

7. Conclusions

An innovative instrument, so-called POLVSM, was developed to measure the multispectral directional and polarized scattering properties of marine particles. The POLVSM instrument could be used as a benchtop instrument onboard a ship or at laboratory. The output data consists of the elements of the 3x3 Mueller scattering matrix, which links the light scattered by the hydrosols with the incident beam. The POLVSM instrument uses a single detector that rotates around the water sample. Many original features of the POLVSM device were described along the paper. First, the range of scattering angles that is covered by the detector is sufficiently wide, namely from 1° to 179°, to permit analysis of the forward and backward directional effects of hydrosols. Such a wide coverage of scattering angles could be obtained due to an original concept based on an optical periscope. Due to the periscope, the laser sources do not obstruct the signal received by the detector. One of the most striking features of the periscope relies on the design of a custom made prism, whose role is to prevent any stray light that could be specularly reflected by the prism toward the receiver. As a result, the detector only measures the scattering properties of the hydrosols. It is thus not necessary to apply any *a posteriori* correction of the signal received. Note that the prism could be used for developing optical instruments beyond the scope of oceanography research field. Another interesting feature of the POLVSM device is its ability to measure the polarization scattering properties of the marine particles. Rotating polarizers are placed both in front of the light source and the detector to derive the Mueller scattering matrix elements. Note that the term V of the Stokes vector is not currently measured with POLVSM instrument.

Relevant and rigorous approaches for the data processing and the calibration procedure of the instrument were proposed to obtain good quality data. The data processing mainly consisted of using the Stokes formalism to derive the Mueller matrix elements (e.g., recomposition of the signal measured for each configuration of the polarizers, attenuation and scattering volume correction). The calibration method consists of converting the output raw signal measured by the detector into geophysical units (namely m^{-1} sr^{-1}). For that purpose, microsphere beads for which the refractive index, the density and the size are accurately known were employed. Mie theory was used to calculate exactly the expected scattering coefficient. Calibration experiments were carried out for various sizes and concentrations of beads to provide a relative uncertainty in the POLVSM data. The results showed that the volume scattering function is measured within ± 4.3% which is highly satisfactory considering the various potential sources of errors that could alter the measurements of the VSF with nephelometers. The consistency of the angular structure of the POLVSM measurements with theory was verified as well. The efficiency of the custom-made prism to remove stray light in the backward direction was demonstrated. Note that the calibration procedure proposed in this paper could be applied to perform the required corrections of the signal measured by other instruments.

Finally, the POLVSM instrument was used to characterize the directional and polarized scattering properties of both mineral-like and phytoplankton dominated hydrosols under controlled laboratory measurements. The experimental results showed a fairly flat angular shape of the VSF at backward direction for the sample containing inorganic hydrosols. In opposite, a sharp increase (more than one order of magnitude) was observed for the sample containing biogenic hydrosols. The values of the backscattering ratio were 1.2% and 0.4% for inorganic and biogenic particles respectively. These values were found to be consistent with the literature. The measurements of the maximum degree of polarization highly differ for each type of sample; the maximum value reaches ~50% and ~80% for inorganic and biogenic hydrosols. These data were consistent as well with both the literature and theoretical considerations arguing that the degree of polarization decreases with increasing refractive index. The good performance of POLVSM instrument was thus verified. The comparison of our experimental results with Mie theory using realistic model inputs revealed that the VSF

#220922 - $15.00 USD Received 13 Aug 2014; revised 9 Oct 2014; accepted 9 Oct 2014; published 17 Oct 2014

and degree of polarization data of inorganic hydrosols match very nicely with Mie calculations in spite of their non sphericity features. It was suggested that the homogeneous internal structure of such inorganic hydrosols and their random orientation in space could make them optically equivalent to spheres. Strong discrepancies were observed between data and simulations for the biogenic hydrosol sample (i.e., a difference by one order of magnitude for the backscattering ratio and by a factor of 2 for the degree of polarization). The reconciliation between measurements and Mie calculations is a challenging task for phytoplankton species. It was suggested here that, in addition to the cause of non sphericity of the particles, the heterogeneity of the internal structures of living phytoplankton cells could be the major reason for which the VSF and the degree of polarization are not well retrieved with Mie theory. More sophisticated numerical tools for modelling the internal structures of biogenic particles are required to reproduce and to better understand the directional and polarized scattering processes affecting the light inside the phytoplankton cells.

The results obtained in this study demonstrated the relevance of performing angularly resolved measurements of the Mueller scattering matrix to gain understanding on the mechanisms involved in the scattering of light in the ocean. The indirect implications for the signal reaching the sea surface and *in fine* for satellite remote sensing purposes are important.

Appendix: System of equations used to derive the Mueller matrix elements (in relation with section 3.1)

In this appendix, italic symbols are used for scalar variables and boldface letters are used to represent vectors and matrices. The objective is to determine the nine elements of a sample Mueller matrix M of Eq. (7) through a sequence $N_p \times N_a$ polarimetric measurements, where N_p and N_a are the number of orientation used for PSG and PSA, respectively. Combining Eqs. (7) and (8) (see section 3.1), the sequence of measurements of the scalar radiance I leads to the following system of $N_p \times N_a$ matrix equations [Eq. (23)]:

$$\begin{cases} I\left(\theta_{a1},\theta_{p1}\right) = \begin{pmatrix} 1 & \cos 2\theta_{a1} & \sin 2\theta_{a1} \end{pmatrix} \mathbf{M} \begin{pmatrix} \left(1-\cos 2\theta_{p1}\right) \\ \cos 2\theta_{p1}\left(1-\cos 2\theta_{p1}\right) \\ \sin 2\theta_{p1}\left(1-\cos 2\theta_{p1}\right) \end{pmatrix} \\ \vdots \\ I\left(\theta_{ai},\theta_{pj}\right) = \begin{pmatrix} 1 & \cos 2\theta_{ai} & \sin 2\theta_{ai} \end{pmatrix} \mathbf{M} \begin{pmatrix} \left(1-\cos 2\theta_{pj}\right) \\ \cos 2\theta_{pj}\left(1-\cos 2\theta_{pj}\right) \\ \sin 2\theta_{pj}\left(1-\cos 2\theta_{pj}\right) \end{pmatrix} \\ \vdots \\ I\left(\theta_{aN_a},\theta_{pN_p}\right) = \begin{pmatrix} 1 & \cos 2\theta_{aN_a} & \sin 2\theta_{aN_a} \end{pmatrix} \mathbf{M} \begin{pmatrix} \left(1-\cos 2\theta_{pN_p}\right) \\ \cos 2\theta_{pN_p}\left(1-\cos 2\theta_{pN_p}\right) \\ \sin 2\theta_{pN_p}\left(1-\cos 2\theta_{pN_p}\right) \end{pmatrix} \end{cases} \quad (23)$$

where θ_{ai} and θ_{pj} are the orientation angles of the i^{th} configuration of the polarization state analyzer (PSA) and the j^{th} configuration of the polarization state generator (PSG), respectively. This system of equation can be reformulated in the mathematical formalism used for matrix, as follows [Eq. (24)]:

#220922 - $15.00 USD Received 13 Aug 2014; revised 9 Oct 2014; accepted 9 Oct 2014; published 17 Oct 2014

$$\begin{bmatrix} I(\theta_{a1},\theta_{p1}) & \cdots & I(\theta_{a1},\theta_{pj}) & \cdots & I(\theta_{a1},\theta_{pN_p}) \\ \vdots & \ddots & & \iddots & \vdots \\ I(\theta_{ai},\theta_{p1}) & \cdots & I(\theta_{ai},\theta_{pj}) & \cdots & I(\theta_{ai},\theta_{pN_p}) \\ \vdots & \iddots & & \ddots & \vdots \\ I(\theta_{aN_a},\theta_{p1}) & \cdots & I(\theta_{aN_a},\theta_{pj}) & \cdots & I(\theta_{aN_a},\theta_{pN_p}) \end{bmatrix} = \begin{bmatrix} \mathbf{a}(\theta_{a1}) \\ \vdots \\ \mathbf{a}(\theta_{ai}) \\ \vdots \\ \mathbf{a}(\theta_{aN_a}) \end{bmatrix} \mathbf{M} \begin{bmatrix} \mathbf{p}(\theta_{p1}) & \cdots & \mathbf{p}(\theta_{pj}) & \cdots & \mathbf{p}(\theta_{pN_p}) \end{bmatrix} \tag{24}$$

The dimensions of each matrix are [Eq. (25)]:

$$\mathbf{I_{sys}}\left(N_a \times N_p\right) = \mathbf{A_{sys}}\left(N_a \times 3\right)\mathbf{M}\left(3\times 3\right)\mathbf{P_{sys}}\left(3\times N_p\right) \tag{25}$$

If $N_p \geq 3$ and $N_a \geq 3$, all the nine elements of the considered Mueller matrix can be determined. The optimal (least-squares) polarimetric data reduction equation for **M** uses the pseudo-inverse of $\mathbf{A_{sys}}$ and $\mathbf{P_{sys}}$. The polarimetric data reduction equation is then [Eq. (26)]:

$$\hat{\mathbf{M}} = \left(\mathbf{A_{sys}^t A_{sys}}\right)^{-1} \mathbf{A_{sys}^t I_{sys} P_{sys}^t}\left(\mathbf{P_{sys} P_{sys}^t}\right)^{-1} \tag{26}$$

As a consequence, the procedure readily treats overdetermined measurement sequences (more than nine measurements for the 3×3 Mueller matrix), providing a least-squares solution. In the case of the POLVSM configuration, $N_p=3$ and $N_a=3$. The preceding equation can thus be simplified [Eq. (27)]:

$$\hat{\mathbf{M}} = \mathbf{A_{sys}^{-1} I_{sys} P_{sys}^{-1}} \tag{27}$$

Acknowledgments

The authors are grateful to the French space agency (CNES), the Université Pierre et Marie Curie, the Institut Universitaire de France and the CNRS for funding the project "POLVSM". We are grateful to the staff of the optical/mechanical department of the Observatoire Océanologique de Villefranche (Edouard Leymarie, Eric Tanguy, Dominique Delhommeau) and of the Observatoire Côte d'Azur (Alain Roussel, Paul Girard, Serge Bonhomme) for their contribution to the fabrication of the mechanical pieces of the instrument. We wish to thank Francois Roullier and Sophie Marro, for their great help about the cultures of phytoplankton species. The reference of the patent of the prism P2 described in this paper [Fig. 2] is FR2936871. We would like to thank the anonymous reviewers for their relevant comments and suggestions.

#220922 - $15.00 USD Received 13 Aug 2014; revised 9 Oct 2014; accepted 9 Oct 2014; published 17 Oct 2014